TCAD Simulation Framework of Gas Desorption in CNT FET NO2Sensors

TCAD Simulation Framework of Gas Desorption in CNT FET NO_2 sensors

Stefania Carapezzi, Susanna Reggiani, *Member, IEEE,* Elena Gnani, *Senior Member, IEEE,* and Antonio Gnudi, *Member, IEEE,*

***Abstract*—A TCAD simulation framework of gas desorption induced by self-heating in CNT FET gas sensors is presented. Its key feature is the use of temperature profiles extracted from electrothermal simulations to determine the change of the effective gas-induced doping concentration during the gas desorption phase. The approach allows to investigate the impact of geometrical and physical parameters, in particular the ones related to contacts, on the self-heating desorption process. The main conclusion is that, due to the non-uniform self-heating temperature profile, the near-threshold part of the IDS-VGS curves recover their pristine aspect faster than the rest of the characteristics.**

***Index Terms*—carbon nanotube, CNT FET sensor, gas desorption, electrothermal simulation, technology computer-aided design (TCAD) modelling.**

I. Introduction

CONDUCTOMETRIC gas sensors based on semiconducting metal oxides are widely investigated [1] due to their low cost, simplicity and range of detectable gases. However, these devices need high temperatures because of 1) their working principles and 2) their recovery procedures, which occur through the gas desorption mediated by temperature. All this makes solid-state gas sensors high-power consumption (mW-range) devices, in contrast with the current trend for development of power-saving devices. Carbon nanotubes (CNTs) are envisaged to be a possible solution for low-power gas sensors, given their sensitivity to gas at room temperature [2]. Moreover, it has been demonstrated [3] that the ultra low-power (2.9 μW at V_{DS} of -1.3 V) process of CNT self-heating is enough for the recovery of CNT field effect transistors (FET) used for gas sensing. In fact, a single walled CNT represents an almost ideal low-power heating wire given its minuscule heat capacity and volume, allowing the Joule heat to be generated at very low power dissipation.

A better understanding of self-heating in CNT-based FETs is thus mandatory for the optimization of these devices. In this respect, the use of technology CAD (TCAD) tools to perform electrothermal simulations is particularly attractive. Some results have already been published [4] showing that the TCAD drift-diffusion approach is successful in simulating CNT FET gas sensors. However, currently a TCAD model to mimic the effect of gas desorption under self-heating conditions is still missing. The aim of the present work is to provide an approach in order to emulate the resetting procedure of CNT gas sensors. The key feature of the procedure is the use of temperature profiles extracted from electrothermal simulations to determine the change during the desorption process of an effective doping concentration that mimics the gas-induced charges. Our results show that the change of doping concentration is not uniform along the CNT, and shed light on the impact of this change in the different regions of the CNT on the I-V characteristics.

S. Reggiani, E. Gnani and A. Gnudi are with University of Bologna (ARCES - DEI), V.le Risorgimento 2, 40136 Bologna, Italy e-mail: (antonio.gnudi@unibo.it).

S. Carapezzi was formerly with University of Bologna (ARCES), V.le Risorgimento 2, 40136 Bologna, Italy. Currently she is with Microelectronics Department, CNRS-LIRMM, 34095 Montpellier, France.

Manuscript received xxx, 2017; revised xxxx.

II. Electrothermal Simulations of CNT-based sensor for NO_2

Fig. 1 illustrates the structure of the simulated CNT FET, which is inspired to the experimental devices of [5]. Please refer to the figure caption for geometrical details. Simulations have been performed by means of Sentaurus SDevice [6]. The CNT is modeled with a cylinder of 2-nm diameter made of a semiconducting material having physical parameters chosen so as to mimic a zig-zag (26, 0) CNT. In particular, the (26, 0) CNT density-of-states (DOS) for electrons can be approximated by [7]

$$\mathrm{DOS}_{\mathrm{CNT}}(E) = \frac{8}{\pi a t \sqrt{3}} \sum_i \frac{E}{\sqrt{E^2 - E_{\mathrm{Ci}}^2}} \times \Theta\left(E - E_{\mathrm{Ci}}\right), \tag{1}$$

where Θ is the Heaviside function, $t = 2.7$ eV the nearest neighbor atom hopping energy, $a = 0.246$ nm the lattice spacing and E_{Ci} the edge of the i-th conduction subband. We consider only the first two conduction subbands and symmetrically the first two valence subbands, with $E_{\mathrm{C1}} = \frac{E_{\mathrm{G}}}{2}$

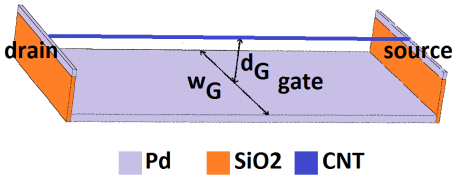

Fig. 1. Scheme of the CNT FET device. A CNT of 2-nm diameter and 2-μm length is suspended across two pillars. Each pillar is made of a layer of silicon dioxide (thickness 240 nm), with a 40-nm thick layer of palladium. Between the two pillars and at their bottom, another 40-nm thick layer of Pd lies, making $d_G = 240$ nm. The space around the CNT and up to d_G nm above it is filled with an insulating material (relative permittivity equal to 1; air). After [5], the metal layers on top of the oxide pillars are biased at the same external voltages than the correspondent contacts at the ends of the CNT.

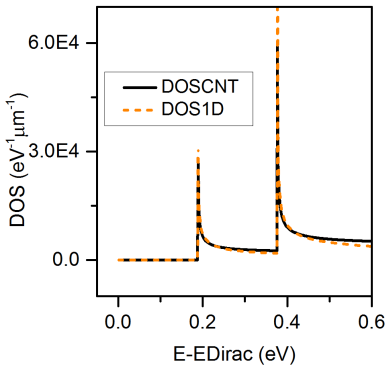

Fig. 2. The black solid line shows the first two subbands above the Dirac energy of $\mathrm{DOS_{CNT}}$ (1) of a zig-zag (26, 0) CNT. The dashed orange line represents the first two subbands of $\mathrm{DOS_{1D}}$ (2), integrated over the cylinder cross-section of a semiconductor wire having the same energy gap and effective mass of the CNT first subband.

and $E_{C2} = E_G$, with the band gap $E_G = \frac{2at}{\sqrt{3}d} = 0.3767\,\mathrm{eV}$, being $d = 26\,a/\pi$.

In order to mimic the CNT DOS within the TCAD simulator, the SDevice Multivalley 1D DOS model is used, using the option `dospower` = -0.5, reading for electrons

$$\mathrm{DOS_{1D}}(E) = \sum_i \frac{\sqrt{2m_i}}{\pi\hbar} \times \frac{1}{\sqrt{E - E_{\mathrm{Ci}}}} \times \Theta\left(E - E_{\mathrm{Ci}}\right), \quad (2)$$

where m_i is the effective mass of the i-th subband. The values $m_1 = 0.23$ and $m_2 = 0.55$ have been used for best fitting of the CNT DOS (1). The $\mathrm{DOS_{CNT}}$ and the TCAD $\mathrm{DOS_{1D}}$ have been plotted in Fig. 2 for comparison purpose. For the source/drain contacts, the SDevice Schottky contact model with contact recombination velocity for electrons and holes and contact resistance has been used. The contact areas coincide with the circular cross-sections at the two CNT ends. The workfunction of graphene (4.55 eV) [8] has been used for the CNT, while the workfunction of Pd has been set to 4.9 eV, resulting in a slightly negative Schottky barrier for holes equal to -0.16 eV. It has been demonstrated in [4] that the experimental transfer characteristics at different V_{SD} of a CNT FET sensor exposed to different gas concentrations

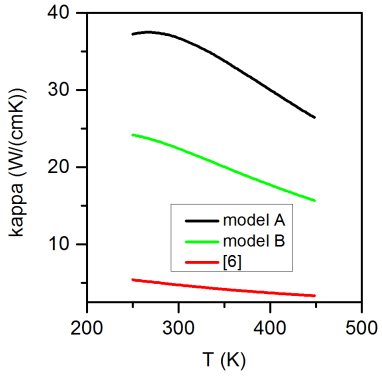

Fig. 3. Empirical models of CNT thermal conductivity.

can be successfully reproduced, provided four parameters are calibrated as a function of the gas concentration, namely the Schottky contact recombination velocity and resistance, as well as the CNT uniform channel mobility and effective doping concentration.

As far as electrothermal simulations are concerned, a dedicated Physical Model Interface (PMI) has been used to implement the following CNT thermal conductivity empirical model (hereafter indicated as model A)

$$k(T) = (a_1 T + a_2 T^2 + a_3 T^{-2})^{-1} \quad (3)$$

where $a_1 = 3.2 \times 10^{-5}$ cm/W, $a_2 = 9.7 \times 10^{-8}$ cm/(W K) and $a_3 = 8 \times 10^2$ cm K^3/W. Eq. 3 is a simplified version of a model of CNT thermal conductivity presented in [9]. In particular, we have considered the limit of infinite channel length. A slightly different empirical model has been found in [10], whose functional dependence on T can still be described by (3), provided parameters a_i, with $i = 1, 2, 3$, are conveniently adjusted. Both models are shown in Fig. 3, together with a third model (hereafter indicated as model B), obtained from model A by changing the value of a_1 into 9×10^{-5} cm/W. The thermal conductivity of model B lies somewhat in between model A and [10]. Both models A and B have been used in the electrothermal simulations discussed in the next paragraphs in order to investigate the sensitivity of the results on the value of the thermal conductivity. Neumann boundary conditions for the temperature have been imposed at the lateral and top boundaries of the air layer. The metal gate underneath the CNT is maintained at room temperature with zero thermal

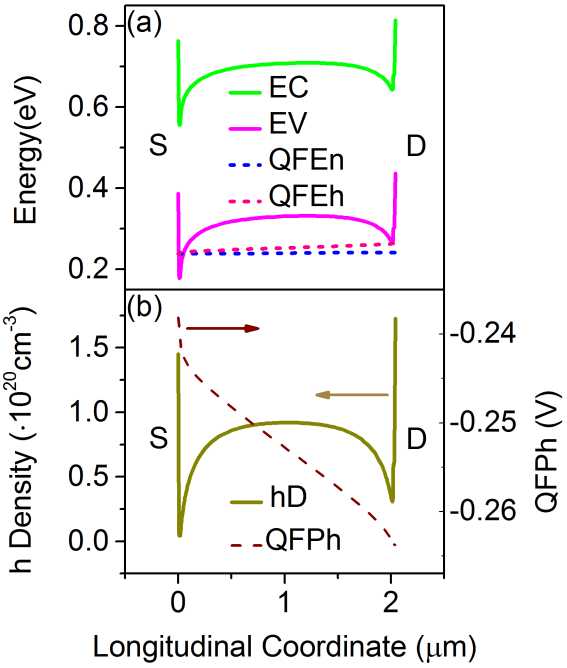

Fig. 4. (a) Band diagram, along the CNT axis, in the active region (VGS = -5V) for the first case study device; VDS = -0.5V. EC and EV are the conduction and the valence band edges, while QFEn and QFEh are the Quasi Fermi Energies for electrons and holes. (b) Hole carrier density and hole Quasi Fermi Potential (QFPh) in the active region (VGS = -5V).

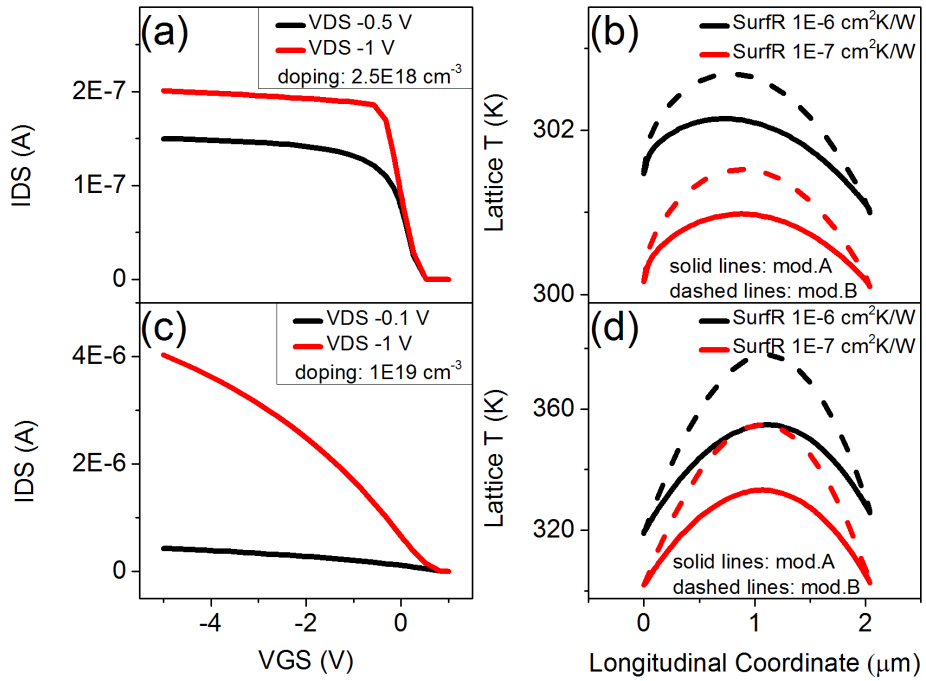

Fig. 5. (a), (c) Simulated IDS-VGS curves after 1-ppm NO_2 exposure. (a) The Schottky contact recombination velocity and resistance, the channel mobility and effective doping concentration are taken from [4]. Black line: VDS = -0.5 V; red line: self-heating condition at VDS = -1.0 V. (c) Same parameters as in (a), but with an infinite contact recombination velocity and a contact resistance of 50 kΩ. Black line: VDS = -0.1 V; red line: self-heating condition at VDS = -1.0 V. (b), (d) Temperature profiles along the CNT axis, extracted from simulations at VDS = -1 V and VGS = -1 V. Thermal conductivity model A (solid lines) and model B (dashed lines) have been considered. For each case, two values of contact thermal surface resistance (SurfR) have been used: 10^{-6} cm^2K/W (black lines) and 10^{-7} cm^2K/W (red lines). In (b) the other model parameters are as in (a); in (d) as in (c).

contact resistance, while for the source/drain contacts room temperature is imposed for the metals, but a non-zero surface thermal resistance is used. Simulations have been performed with two values of surface thermal resistance to account for some variability, namely 10^{-6} cm^2K/W and 10^{-7} cm^2K/W (after [9]).

Two case studies have been considered. In both cases the geometry is the one illustrated in Fig. 1. In the first case the Schottky contact recombination velocity for both electrons and holes is 2.2×10^6 cm/s, the contact resistance is 1.5 MΩ, the electron and hole mobilities are both equal to 4×10^3 $cm^2/(Vs)$ and the uniform effective p-doping density is 2.5×10^{18} cm^{-3}. Such parameters have been taken from [4] and correspond to 1-ppm NO_2 concentration. In Fig. 4(a) is plotted the band diagram along the CNT axis at VGS = -5V (active region), VDS = -0.5 V. The conduction band edge EC and the valence band edge EV at the contacts are determined by the contacts voltage and by the Schottky contacts barriers. The hole barrier strongly favors hole injection, while the electron barrier tends to suppress the electron injection. In a narrow region close to the contacts the band edges relax due to the screening effect of the underneath metal layers, which rest on top of the two oxide pillars (see Fig. 1). Besides these thin regions near the contacts the gate effect dominates and reaches its maximum strength in the middle of the channel. This picture is consistent with the hole density p and the hole Quasi Fermi Potential (QFPh) shown inFig. 4(b), for VGS = -5V, VDS = -0.5 V. At source contact p is less than the equilibrium hole concentration (fixed by the barrier height) p_0, while at drain contact it is greater than p_0, because the recombination velocity is finite. Then the hole density tends to relax to the intrinsic concentration in the narrow region close to the contacts, while it rises in the middle part of the channel. Consequently, the QFPh has a larger gradient near the contacts (in particular at the source) than in the middle of the channel.

The resulting IDS-VGS characteristics at VDS = -0.5 V are shown in Fig. 5(a) (black line). Simulated currents of the same device at VDS = -1 V are also shown in the same figure (red line), corresponding to the self-heating condition. The temperature profiles along the CNT axis calculated with the electrothermal simulations at VGS = VDS = -1 V are shown in Fig. 5(b). Both thermal conductivity models A and B have been employed, as well as the two above mentioned values of contact thermal resistance. The maximum temperature, which occurs around the center of the CNT, is only about 303 K. The reason for such low temperature is the small current value, which is limited by contact effects due to the large electrical contact resistance and finite recombination velocity, as discussed in [4]. This makes the heat generated by Joule effect not high enough to produce a significant increase in the CNT temperature.

In the second investigated case, an infinite contact recombination velocity (thus imposing equilibrium electron and hole concentrations at the contacts) and a contact resistance of 50

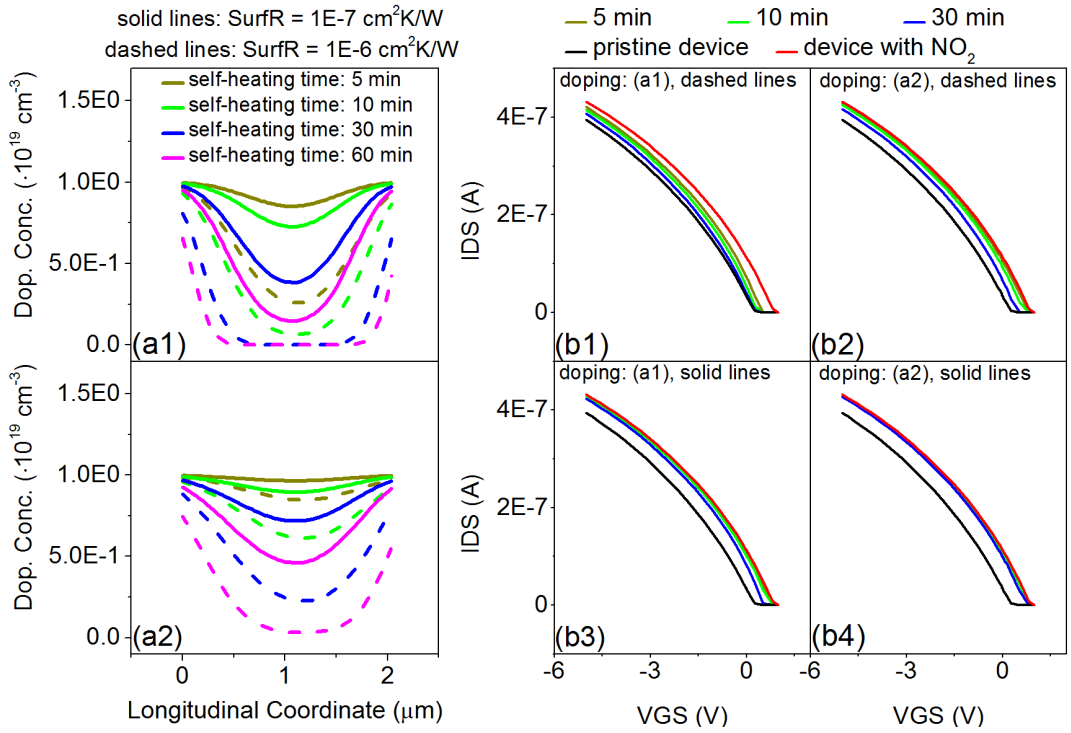

Fig. 6. (a1), (a2) Effective doping profiles along the CNT axis computed at different times after the start of the self-heating process. The temperatures used to calculate them have been extracted by a thermal simulation using I) model A of thermal conductivity, II) contact surface thermal resistance of 10^{-6} cm^{2}K/W (dashed lines) and of 10^{-7} cm^{2}K/W (solid lines), III) doping concentration of (a1) 10^{19} cm^{-3} and (a2) 0. (b1) - (b4) Simulated IDS-VGS curves (VDS = -0.1V) after 5 (green lines), 10 (blue lines) and 30 (cyan lines) minutes from the beginning of self-heating. The doping densities of (a1) have been used in (b1) (doping: dashed lines) and (b2) (doping: solid lines). The doping densities of (a2) have been used in (b2) (doping: dashed lines) and (b4) (doping: solid lines). The currents under pristine condition (black lines) and after exposure to 1-ppm NO_2 concentration (red lines) are also shown for comparison.

kΩ have been considered. Such values have been chosen with the aim of achieving at VGS = VDS = -1 V a value of current (1.7×10^{-6} A) similar to the experimental current (1.6×10^{-6} A) measured in [3] at recovery condition. It should be observed that for the experimental device of [3] self-heating was indeed successfully used to reset the CNT FET. In addition, a uniform p-doping density of 10^{19} cm^{-3} has been used to emulate a threshold voltage shift induced by gas absorption of about 1V. The simulated IDS-VGS characteristics at VDS = -0.1 V and VDS = -1 V are shown in Fig. 5(c). The simulated temperature profiles in the recovery conditions are shown in Fig. 5(d). Now the maximum temperature, which occurs nearly in the middle of the CNT, ranges from 333 K (for thermal conductivity model A and contact thermal resistance of 10^{-7} cm^{2}K/W) to 377 K (for thermal conductivity model B and contact thermal resistance of 10^{-6} cm^{2}K/W). Understandably, the temperature is larger when a higher contact resistance and a lower thermal conductivity are used.

III. Gas Desorption Model

Under the hypothesis that the contacts are passivated, as was the case in [3], then the effect of gas desorption mainly affects the effective doping. Instead, for unpassivated contacts 1) the gas would be adsorbed also at the contacts, thus changing their properties. Consequently, the contacts would contribute to the sensor response. However, the contacts do not heat up by self-heating because of their heat dissipation, therefore 2) the gas could not be desorbed at the contacts. Hence, the sensor resetting by self-heating would result impossible with unpassivated contacts.

After [11], the following model has been implemented to mimic the change of doping induced by self-heating

$$N(t,\mathbf{r},T) = N_0(\mathbf{r})e^{-t/\tau_{des}(T)} \tag{4}$$

where $N(t,\mathbf{r},T)$ is the effective doping profile within the CNT at time t from the beginning ($t=0$) of the self-heating process, while $N_0(\mathbf{r})$ is the initial doping profile. In our case $N_0(\mathbf{r}) = 10^{19}$ cm^{-3}. The desorption time constant $\tau_{des}(T)$ is given by

$$\tau_{des}(T) = \frac{1}{\nu}e^{-E_b/k_BT} \tag{5}$$

where E_b is the analyte desorption energy barrier, ν the attempt frequency and k_B the Boltzmann constant. $E_b = -1.01$ eV has been taken from [3], while $\nu = 10^{12}$ s^{-1} has been taken from [12]. The model of Eq. 4 and 5 has been indeed tested against experimental data [11]. However, it is a simple picture of the process of gas desorption from CNT surface and other effects, such as possible surface diffusion of molecules from high concentration regions to low concentration regions during the desorption process, have been neglected.

It should be noticed that in Eq. (4) temperature is implicitly assumed to be time-independent, i.e. the temperature profile calculated with a thermal simulation using the effective doping concentration at $t=0$ (10^{19} cm^{-3}) is used for any t. However, the change of doping induced by self-heating indeed affects

the current, and then in turn the temperature generated by Joule effect. Therefore, the use of T extracted by a thermal simulation using a costant doping of 10^{19} cm^{-3} for calculating $N(t, \mathbf{r}, T)$ could lead to some overestimate depending on t. In order to understand the range of variability introduced by this, we have repeated the calculation of $N(t, \mathbf{r}, T)$ by using the T extracted by thermal simulation with zero doping.

Fig. 6(a1) and (a2) shows the computed effective doping profiles at different times after the beginning of the self-heating process. Model A of thermal conductivity and both previously mentioned surface thermal resistance values have been used in the electrothermal simulations. As expected, the desorption effect, i.e. the decrease in doping density, is more relevant where the temperature is higher, that is in the middle of the CNT. Near the two ends of the CNT, i.e. close to the contacts, the heat dissipation is higher and the doping density remains high. Also, the change in doping is more accentuated when the T used for calculation is computed by electrothermal simulations using a doping concentration of 10^{19} cm^{-3} (Fig. 6(a1)) compared to when a zero doping is used (Fig. 6(a2)), especially in the short t range. This is related to the fact that with zero doping the currents are smaller than when doping is 10^{19} cm^{-3}, then the Joule effect is smaller.

It is now interesting to evaluate the effect of the not uniform change of doping density over the IDS-VGS curves. To this end, the computed doping profiles at different time steps of Fig. 6(a1), (a2) have been loaded onto the device geometry file and new TCAD simulations have been performed at VDS = -0.1 V. The results are plotted in Fig. 6(b1) - (b4): doping of panel (a1) has been used as input in simulations of Fig. 6(b1), (b3), while doping of panel (a2) has been used for simulations of Fig. 6(b2), (b4). The currents for the pristine and the 1-ppm NO_2 conditions are also shown for comparison. It is apparent from Fig. 6(b1), (b2) that the near-threshold part of the characteristics tends to recover the pristine condition faster than the high-current part. This can be attributed to the larger sensitivity of the near-threshold current on the doping concentration in the middle of the CNT, which tends to desorb faster (Fig. 6(a1), (a2)). This is confirmed also by the results of Fig. 6(b3), where a partial recover is obtained after 30 min only near threshold. Of course, in this case much longer times are required for a more complete recover, due to the lower temperatures.

IV. Conclusion

TCAD simulations of CNT FET gas sensors have been presented in this letter, coupled with an analytical gas desorption model that uses the temperature profiles extracted from the electrothermal simulations of the CNT during the self-heating process. An effective doping concentration accounts in the TCAD simulation framework for the gas-induced charge in the CNT. The procedure allows to study the impact of the contact electrical and thermal resistance, as well as the CNT thermal conductivity, on the temperature profiles along the CNT and hence on the self-heating desorption process. An interesting conclusion of the present study is that, in spite of the non-uniform gas desorption due to the self-heating temperature peaking near the center of the CNT, the near-threshold part of the IDS-VGS characteristics recovers within a reasonable time to its pristine aspect, as opposed to the high-current part of the curve. Finally, our results confirm the importance of achieving a good control of the electrical and thermal properties of the contacts for reliable sensor operation.

Acknowledgment

The research leading to these results has been supported by the Italian MIUR through EU H2020 FLAG–ERA JTC 2016 project CONVERGENCE "Frictionless Energy Efficient Convergent Wearables For Healthcare And Lifestyle Applications", via the IUNET Consortium. The Authors wish to thank Dr. Cosmin Roman and Mr. Seoho Jung, Micro- & Nanosystems, Department of Mechanical and Process Engineering, ETH Zürich, Swiss, for fruitful discussions.

References

[1] N. Barsan, D. Koziej, and U. Weimar, "Metal oxide-based gas sensor research: How to?" *Sensors and Actuators B: Chemical*, vol. 121, no. 1, pp. 18 – 35, 2007, special Issue: 25th Anniversary of Sensors and Actuators B: Chemical. [Online]. Available: http://www.sciencedirect.com/science/article/pii/S0925400506006204

[2] K. Chikkadi, M. Muoth, C. Roman, M. Haluska, and C. Hierold, "Advances in NO_2 sensing with individual single-walled carbon nanotube transistors," *Beilstein Journal of Nanotechnology*, no. 5, p. 2179–2191, 2014.

[3] K. Chikkadi, M. Muoth, V. Maiwald, C. Roman, and C. Hierold, "Ultra-low power operation of self-heated, suspended carbon nanotube gas sensors," *Applied Physics Letters*, vol. 103, no. 22, p. 223109, 2013. [Online]. Available: https://doi.org/10.1063/1.4836415

[4] S. Carapezzi, S. Eberle, S. Reggiani, E. Gnani, C. Roman, C. Hierold, and A. Gnudi, "3D TCAD modeling of NO_2 CNT FET sensors," in *2018 48th European Solid-State Device Research Conference (ESSDERC)*, 2018, pp. 222–225.

[5] S. Eberle, C. Roman, and C. Hierold, "Effect of varying gate distance on the threshold voltage shift in carbon nanotube field effect transistor gas sensors," *Microelectronic Engineering*, vol. 193, pp. 86 – 90, 2018. [Online]. Available: http://www.sciencedirect.com/science/article/pii/S0167931718300959

[6] *Sentaurus Device User Guide, Version P-2019.03*, Synopsys Inc., Mountain View, CA, USA, 2019.

[7] J. W. Mintmire and C. T. White, "Universal density of states for carbon nanotubes," *Phys. Rev. Lett.*, vol. 81, pp. 2506–2509, Sep 1998. [Online]. Available: https://link.aps.org/doi/10.1103/PhysRevLett.81.2506

[8] W. S. Su, T. C. Leung, and C. T. Chan, "Work function of single-walled and multiwalled carbon nanotubes: First-principles study," *Phys. Rev. B*, vol. 76, p. 235413, Dec 2007. [Online]. Available: https://link.aps.org/doi/10.1103/PhysRevB.76.235413

[9] E. Pop, D. Mann, Q. Wang, K. Goodson, and H. Dai, "Thermal Conductance of an Individual Single-Wall Carbon Nanotube above Room Temperature," *Nano Letters*, vol. 6, no. 1, pp. 96–100, 2006, pMID: 16402794. [Online]. Available: https://doi.org/10.1021/nl052145f

[10] Y. Gu and Y. Chen, "Thermal conductivities of single-walled carbon nanotubes calculated from the complete phonon dispersion relations," *Phys. Rev. B*, vol. 76, p. 134110, Oct 2007. [Online]. Available: https://link.aps.org/doi/10.1103/PhysRevB.76.134110

[11] S.-Z. Liang, G. Chen, A. R. Harutyunyan, M. W. Cole, and J. O. Sofo, "Analysis and optimization of carbon nanotubes and graphene sensors based on adsorption-desorption kinetics," *Applied Physics Letters*, vol. 103, no. 23, p. 233108, 2013. [Online]. Available: https://doi.org/10.1063/1.4841535

[12] S. Peng, K. Cho, P. Qi, and H. Dai, "Ab initio study of cnt no2 gas sensor," *Chemical Physics Letters*, vol. 387, no. 4, pp. 271 – 276, 2004. [Online]. Available: http://www.sciencedirect.com/science/article/pii/S0009261404002398